Oil & Gas Science and Technology – Rev. IFP Energies nouvelles **75**, 5 (2020)

https://doi.org/10.2516/ogst/2019069

Available online at:
ogst.ifpenergiesnouvelles.fr

REGULAR ARTICLE OPEN ACCESS

The effectiveness of computed tomography for the experimental assessment of surfactant-polymer flooding

Fabián Andrés Tapias Hernández*, and Rosângela Barros Zanoni Lopes Moreno

School of Mechanical Engineering, Department of Energy, University of Campinas, Rua Mendeleyev 200, 13083-860 Campinas, São Paulo, Brazil

Received: 22 July 2019 / Accepted: 12 December 2019

Abstract. The Surfactant-Polymer (SP) process is a type of Chemical Enhanced Oil Recovery (CEOR) method. They are still a challenge for the petroleum oil industry mainly because of the difficulty in designing and forecasting the process behavior on the field scale. Therefore, understanding of the phenomena associated with a CEOR process is of vital importance. For these reasons, this work discusses the benefits of Computed Tomography (CT) uses for the experimental assessment of a SP process. The research includes a literature review that allows identifying the main CT usages for petroleum engineering and a discussion concerning the effectiveness of mathematic expressions proposed for the tomography images treatment of two-phase flow displacement. The conducted experimental methodology can be reproduced to assess the benefits of any chemical Enhanced Oil Recovery (EOR) process with CT. Thus, this paper assesses the conventional waterflooding (WF) and SP flooding as secondary and tertiary oil recovery methods. The developed study allowed us to evaluate through CT images the porosity and the saturation profiles along the rock sample. Also, CT processed data enabled checking the volumetric material balance and determine the oil Recovery Factor (RF). The doubled checked SP data showed an RF increase of 17 and 10 percentage points for secondary and tertiary chemical injection schemes respect to conventional waterflooding. Finally, comparative results of the water cut (W_{cut}) evidenced the mobility ratio improvement and reduction on the remaining oil saturation.

1 Introduction

Nowadays, the growing global energy demand and the gradual revitalization of the oil prices [1] stimulate the reactivation of mature oil fields. These fields, usually developed through water or gas injection (secondary recovery methods), require the implementation of some Enhanced Oil Recovery (EOR) technique. Nevertheless, despite the common idea about the application of EOR methods in the advanced stage of the reservoirs life cycle, these techniques can also be utilized at any time during the field development aiming to improve the oil Recovery Factor (RF).

Several authors [2–5] have grouped EOR methods into three broad categories: thermal, miscible and chemical processes. The last group consists of adding chemical products to the fluids injected. One of these methods includes the addition of surfactant products, whose goal is to reduce the interfacial tension, increasing the capillary number and, therefore, decreasing the oil saturation. This method can be applied combined with a polymer solution, as a control mobility agent, looking for an increase in displacement efficiency [6]. This combination of chemical products and mechanisms is known as Surfactant-Polymer (SP) process.

The Chemical Enhanced Oil Recovery (CEOR) processes have been revitalized globally after two decades of relative calm [7]. Among those processes, Polymer Flooding (PF) is the most used method on a field scale, whereas, technical reasons have limited the application of the SP and Alkali/Surfactant/Polymer (ASP) methods. Limiting factors include the difficulty in designing and forecasting the process behavior in the field scale, the excessive formation of carbonate or silicate scale and the formation of stable emulsions in the production facilities. Therefore, these processes still are a challenge for the petroleum industry, and laboratory tests are the first step to improve the understanding of these kinds of methods.

Detailed visualization of the *in-situ* fluids dynamics during core-flooding tests is vital to improving the mechanisms description and the proper process design. For this reason, several authors have presented results including Computed Tomography (CT). They are Batenburg *et al.* (2015) [8], London *et al.* (2014) [9], Hove *et al.* (1990) [10], Hunt *et al.* (1988) [11], Wang *et al.* (1984) [12], Wellington and Vinegar (1987) [13], Vinegar and Wellington (1987) [14], Withjack (1988) [15], Withjack *et al.* (2003) [16],

* Corresponding author: fabian.tapias@hotmail.com

Wan *et al.* (2019) [17], Ouali *et al.* (2019) [18]. It is important to highlight that core-flooding tests allow calibrating field simulation models reducing uncertainties on rock–fluids interactions. Thus, run experiments focused on a target field are essential to forecast of petroleum exploitation strategies.

Based on the above information, this study focused on evaluating the effectiveness of CT for the experimental assessment of a SP injection, as secondary and tertiary oil recovery methods. The imaging technique advantages as a powerful tool to visualize 2D and 3D porous media images are discussed.

1.1 Computed Tomography (CT)

The CT is a radiological imaging technique to take projections from many different angles of a scanned object aiming to reconstruct cross-sectional images of specific areas of it through combinations of many X-ray measurements and computer-processing.

Each reconstructed sectional image is equivalent to a matrix of 512 × 512 values. Each unitary square represents a pixel of the slice. The fundamental quantity measured in each pixel of a CT image is the linear attenuation coefficient, τ, which is defined by the Beer's Law:

$$\frac{I}{I_o} = \exp(-\tau h), \tag{1}$$

where I_o is the incident X-ray intensity and I is the intensity remaining after the X-ray passes through a thickness, h, of a sample [13].

The linear attenuation coefficient depends on both electron density (bulk density – ρ) and the atomic number (Z). Both properties are predominant at different X-ray energies, *i.e.*, the ρ of the materials is predominant at above 100 kV whereas that Z is predominant at below 100 kV. The CT attenuation data are typically presented on a scale called Hounsfield (H) units, that are defined by air at −1000 (H) and water at 0 (H). It is also named as CT number.

CT has proved to be a useful tool for studies of fluids dynamic during EOR process. The evidence is shown below.

Wellington and Vinegar (1987) [13] presented several petrophysical applications, including three-dimensional measurement of density and porosity, rock mechanics studies, correlation of core logs with well logs, characterization of mud invasion, fractures and quantification of complex mineralogies. They also included fundamental studies of CO_2 displacement in cores focusing on viscous fingering, gravity segregation, miscibility and mobility control.

Vinegar and Wellington (1987) [14] presented a review of the principles of CT, explained a method to develop two and three-phase saturation measures based on CT images. They highlighted the importance of a correct choice of dopant products (some chemical products with a high atomic number) to be applied to some of the fluids with the purpose of improving the visualization and differentiate fluids during the core flood process.

Hove *et al.* (1990) [10] showed the visualization of xanthan core-flood using CT. They used sodium iodide (NaI) as aqueous dopant product. Their experiments evaluated the one-phase flow of xanthan solutions and immiscible displacement using light refined oil. Alvestad *et al.* (1992) [19] reported the use of CT for core-flood experiments applying surfactant. The CT data gave valuable information about the flow dynamics and the distribution of the residual oil in the core.

Coles *et al.* (1995) [20] focused on the importance of calibrating or having a reference for CT values during the long experimental process. They presented three different methods used to improve the accuracy and reliability of CT results and showed the importance of these procedures for the calculation of saturation profiles.

Hicks (1996) [21] presented a summary of CT utilities in petroleum engineering and showed the images results of a displacement process using benzyl alcohol, water, and decane to model the oil, water and gas system. Based on this, they observed gravity segregation of the benzyl alcohol, even though the region was in steady-state condition.

Sharma *et al.* (1997) [22] presented a complete report about the use of CT techniques for two-phase and three-phase *in-situ* saturation measurements. They exposed details about the experimental procedures, data acquisition and data processing computer programs. They reduced the error in the computation of saturations, which was mainly generated due to the assumption that X-ray attenuation for a pure component is constant over the complete scan area. Thus, they changed the need for a scan at totally oil saturated rock condition for a scan at a connate water saturation state. This approach was verified by waterflooding experiments with and without dopant products, exhibiting good agreement when existing sufficient difference between the CT values of the fluids used. They indicated 1-Iodododecane as a possible dopant, since it is more efficient to increase the CT attenuation properties of the oil.

Chakravarthy *et al.* (2004) [23] showed CO_2 and WAG flooding experiments in homogenous and fractured rock with *in-situ* saturation and porosity measurements using CT. They presented the experimental process used to develop the tests. The overall efficiency of the process was analyzed by combining the CT measurements and the measurements of effluent volumes.

Berg *et al.* (2010) [24] used the images processing to determine the physics of the experiments by identifying processes like viscous fingering, channeling and gravity segregation impact the recovery efficiency. The link between the 3D imaging and 2D and 3D numerical simulation opens up a route for the determination of parameters as relative permeabilities and capillary pressure in a much more efficient way [25, 26].

1.2 Screening of surfactant-polymer process

Several authors have presented different criteria for the correct selection of a field candidate to apply the SP method. Table 1 summarizes some of these criteria.

Then, we choose San Francisco (SF) field as a reference, since their features satisfied those criteria. The SF field was discovered in 1985 and is located at 20 km northwest of the

Table 1. Screening of an SP process.

Reservoir conditions			Reservoir rock properties				Reservoir fluids properties			Reference
Temperature (°C)	Depth (CD)	Permeability (SSJD)	Porosity (%)	Lithology	Clay	Oil saturation* (fraction)	Water salinity (ppm)	Oil viscosity (cp)	API gravity (°API)	
<90	<6561	>50	>18	Sand and sandstone	Low	>0.4	Low	<30		Carcoana [27]
<93.3	<9000	>40	>20	Sandstone		>0.3	<100 000	<40	>25	Goodlett *et al.* [28]
<93.3	8500	>20		Sandstone	Low	>0.25	<50 000	<20	>25	Brashear and Kuuskraa [29]
<93.3	9000	>10		Sandstone		>0.35		<35	>20	Taber *et al.* [4]
<70		>50		Sandstone	Low	>0.35	<50 000	<150	<35	Al-Bahar *et al.* [30]
<71.1	<4600	>170	>20	Sandstone		>0.6	<150 000	<80	>14	Ezekwe [31]
<93.3		>10		Sandstone	Low	>0.3	<50 000	<35		Sheng [32]
<70	NC$^+$	>10	>18	Sandstone	Low	>0.25	<50 000	<35	NC$^+$	Proposed in this work

Oil saturation*: Before SP, NC$^+$: No critical variable.

Table 2. Rock samples petrophysics characterization.

Rock sample	Type	Porosity (%)	Permeability (mD)
12A2	Sandstone	23.41	435.32
12A4	Sandstone	23.82	534.52

city of Neiva in the Upper Magdalena Basin (Colombia). The Cretaceous Upper Caballos Formation is the leading producer unit of the SF field. It formation consists of coarse to fine-grained quartz sandstones in an estuarine environment and contains 75% of the Stock Tank Original Oil In Place (STOOIP). The SF field is an example of a mature field producing under a mature waterflooding project, at water cut higher than 90% and an unfavorable mobility ratio [33]. The reservoir is considered preferentially water-wetting, the temperature is 50 °C, with an initial pressure of 1100 (Psia) at a depth of 3000 (ft), a permeability and porosity range of 20–2000 (mD) and 12–23%, respectively and a residual oil saturation is closer than 0.25. The oil viscosity was determined at reservoir temperature and corresponds to 18.4 (cp). The cations brine equivalent to SF composition corresponds to 7093 ppm of NaCl.

It is important to highlight that the reported information is only a reference for the properties to be experimentally recreated to develop this work.

2 Material and procedures

2.1 Rock samples

Sandstone samples with a diameter of 3.8 cm and length of 27 cm of Botucatu Formation, located in Ribeirão Claro at Paraná Sedimentary basin, were selected. These rock samples were characterized by permeability values below 1000 mD and porosities between 22% and 24%, values closer to target conditions. Then, methanol and toluene were displaced throughout the rock samples aiming to remove the organic and inorganic compounds. After cleaning and drying the rock samples, the petrophysical properties were measured. Table 2 shows the results.

The dry rock samples were placed inside the core holder and submitted to an overburden pressure, and then, a CT scan was run to determine some internal rock characteristics [34].

2.2 Synthetic brine

Density and viscosity of the Synthetic Brine (SB) containing 7093 ppm of dissolved NaCl were measured at atmospheric pressure and a temperature of 50 °C to be 0.990 (g/cm^3) and 0.6 (cP), respectively.

2.3 Oil

The oil used was a mixture of Field dehydrated oil (69% wt), Kerosene (21% wt) and Iododecane (10% wt). The mixture density and viscosity were measured to be 0.916 (g/cm^3) and 18 ± 1 (cP), respectively, at atmospheric pressure and a temperature of 50 °C.

It is relevant to highlight that iodized oil (Iododecane – I_{10}) was selected as a dopant product to improve the visualization of the oil phase flow by CT acquisition.

2.4 Polymer and surfactant

The polymer selected was the Synthetic HPAM, Flopaam 3230S from *SNF Floerger* with a molecular weight (Mw) of 5×10^6 (g/mol), 30% degree of hydrolysis, water content less than 1% [35]. Besides that, the Sodium Dodecyl Sulfate (SDS) from LabSynth with Mw of 288.373 (g/mol) and a purity of 99.23% was selected as a surfactant.

This polymer was chosen because the molecular weight of HPAM has a direct relationship with the permeability of the porous media through the polymer will be injected [2]. On the other hand, the SDS was already evaluated as a useful chemical for a CEOR process with a similar oleic phase composition [36].

2.5 Fluids preparation

The preparation of the SP blend solutions differs from the process exhibited in the API RP 63 [37] only by the composition of the solution used to prepare the polymer stock solution. In this case, a mixture of brine and surfactant was used. Therefore, a stock HPAM solution containing 5000 ppm of the polymer was prepared using the synthetic brine previously described.

The SB was deaerated utilizing a vacuum pump. These HPAM solutions were agitated using a magnetic stirrer during 5–7 h to form a consistent solution, *i.e.*, the solution exhibited a homogeneous aspect, and it did not have insoluble particles (fisheye). All of the HPAM solutions were prepared carefully with the minimum agitation (80 rpm) to avoid the mechanical degradation of the long-chain molecules. The stock solutions were left still overnight to ensure full hydration.

Then, HPAM stock solutions were diluted with SB up to the desired concentration. The new solution was put into a beaker and homogenized by magnetic stirrer at low speed (80 rpm) for 10 min. All HPAM solutions were stored in closed recipients to minimize oxygen uptake.

The fluids properties and phase behavior of these aqueous solutions were studied previously by the authors [38].

2.6 Bulk fluids CT values determination

To know the bulk fluids CT values is necessary to reduce numerical errors at experimental conditions due to the assumption of the monochromatic X-ray nature during the determination of porosity and saturation profiles using CT images.

For this, an annular cylinder drilled from aluminum rods (OD: 3.8 cm, ID: 1.8 cm, length: 12 cm, $\tau_{\text{aluminum}} = 1774.4$ [H]) was used. This device was placed inside the core holder, pressurized at 3000 (psi), heated at 50 °C and filled with the fluids at the conditions mentioned previously. Then, CT scans were conducted to determine the attenuation coefficient values for synthetic brine (116.4 [H]), oil (570.8 [H]), nitrogen (−808.8 [H]) and air (−796.8 [H]) at 50 °C and atmospheric pressure.

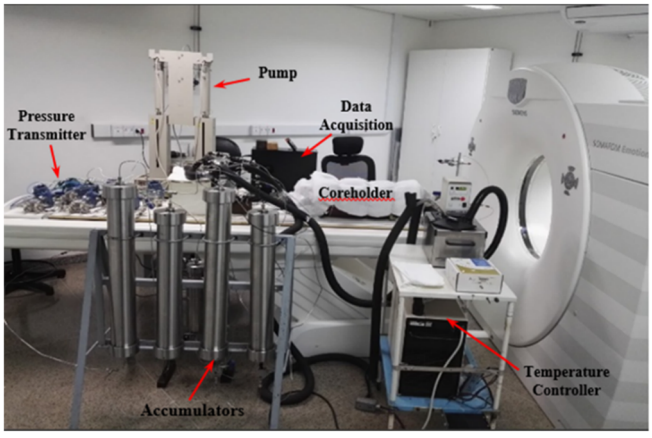

Fig. 1. Real core flood assembling.

2.7 Core flood assembling

The experimental bench includes two accumulators filled with mineral oil to be used as a hydraulic piston for the fluids to be injected. Besides that, the assembling has a thermal bath to heat up the liquids before these come into the core holder up to 50 °C. A resistance heating jacket envelops the core holder to maintain water temperature in the annular space between the rubber that covers the rock and the core holder at 50 °C, approximately. Finally, assuming that the heat loss between the water and the rock is negligible, we can consider that the process is carried out under isothermal conditions. Figure 1 shows the final setup used for the core-flooding tests.

Also, six pressure transmitters were used connected in parallel (3 of 9 psi and 3 of 300 psi). These connections were set because the Differential Pressure (DP) expected during the imbibition 1 (K_w estimative) is smaller or closer than one psi, while for the other stages, the awaited DP is closer or higher than 9 psi. One of these sensors captures the DP across the total sample, *i.e.*, between the inlet face and the output face of the rock, and the others are responsible for registering two different differential pressures along the rock sample. Since the core holder containing the rock sample is positioned on the tomography bed, it cannot move. This condition is needed because the image treatment is based on mathematic operations using the same scanned positions acquired at different instants during the core-flooding.

2.8 Core-flooding tests

This research encompasses three different core-flooding experiments evaluated by CT. The first test was designed to recreate the oil recovery process by water injection. The second one aims to analyze the oil recovery using a continuous flood of a tailor-made SP blend through the rock at initial reservoir condition (S_{wi} – Initial Water Saturation and S_o – High Oil Saturation), *i.e.*, in this case, the SP process is studied as a secondary oil recovery method. Finally, the third test aims to assess the performance of the same SP blend solution as a tertiary oil recovery method, *i.e.*, Chemical injection starts when the oil saturation into the rock is

close to the oil residual value (S_{or}). Table 3 shows the preliminary planning.

Tests 1 and 2 were conducted in the same rock sample (12A4) as a continuous process, and we assumed that the petrophysical properties after waterflood were the same. Thus, Test 2 was performed after oil re-saturation of the rock sample (Drainage 2), which was conducted injecting oil phase up to the pressure stabilizes. The injection flow rate was chosen within the stability flood criteria proposed by Dos Santos *et al.* [39].

The rock samples were not aging aiming to preserve the water-wet nature of the Botucatu rock samples [40] through the cleaning process and thus, keeping a similar wettability condition respect to the reference field selected.

In Test 2, the target was the maximum oil production using the SP blend as a secondary recovery method. Therefore, it was considered necessary to reach stabilized conditions on differential pressure and null oil production. This approach allowed to determine the amount of SP blend, that was necessary to obtain the largest incremental oil respect to

Table 3. Experimental planning to core-flooding tests.

Feature/Step	Test 1	Test 2	Test 3
Kind of test	Waterflooding	SP as secondary method	SP as tertiary method
Core sample	12A4	12A4	12A2
Porosity (%)	23.82	23.82	23.41
Permeability (mD)	534.52	534.52	435.32
PV (cm^3)	72.58	72.58	68.58
Injection rate (cm^3/min)	0.5	0.5	0.5
Imbibition 1	Brine	–	Brine
Drainage 1	Oil		Oil
PV_{inj}	7	–	7
Fluid quantity (cm^3)	508.03		480.03
Waterflooding	Brine		Brine
PV_{inj}	15	–	7
Fluid quantity (cm^3)	1088.65		480.03
Drainage 2		Oil	
PV_{inj}	–	7	–
Fluid quantity (cm^3)		508.03	
CEOR 1			
SP Injection 1		Blend HPAM 2000 ppm + 0.5 [%wt] SDS	Blend HPAM 2000 ppm + 0.5 [%wt] SDS
Viscosity at 7.3 S^{-1} and 50 °C (cP)	–	10	10
PV_{inj}		10	0.7
Fluid quantity (cm^3)		725.8	48.00
Drive		Brine	Brine
PV_{inj}	–	5	4
Fluid quantity (cm^3)		362.9	274.31
CEOR 2			
SP injection 2			Blend HPAM 2000 ppm + 0.5 [%wt] SDS
Viscosity at 7.3 S^{-1} and 50 °C (cP)	–	–	10
PV_{inj}			0.5
Fluid quantity (cm^3)			34.29
Drive 2			Brine
PV_{inj}	–	–	4
Fluid quantity (cm^3)			274.31

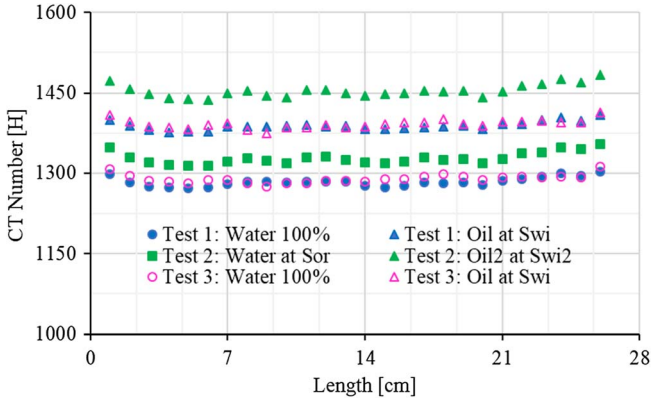

Fig. 2. CT profiles of reference media for each step of the tests.

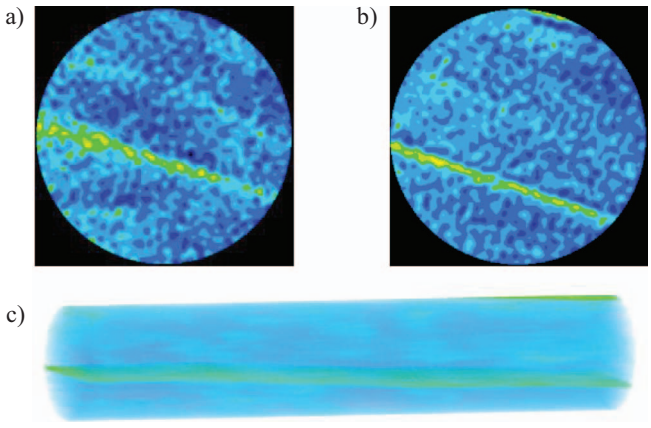

Fig. 3. Initial CT analysis of dry rock sample 12A4. Slices 6 and 20 along the rock, respectively (a and b), and 3D reconstruction of the entire rock sample, where the green color represents the laminations and high-density materials (c).

the WF process. This amount corresponds to the inflection point in Figure 21. After the chemical flooding, the injection of additional five Pore Volumes (PV) of chase water confirmed the absence of incremental oil production.

In Test 3, the chemical amount was dimensioned based on the results of Test 2. Thus, SP blend amounts of 0.7 and 0.5 PV were injected in each slug of the designed CEOR processes. The post flush with water was dimensioning aiming to guarantee a similar amount of injected fluid aiming to compare the performance of both processes (Test 2 and Test 3).

2.9 Data imaging

The CT scanner Somatom Emotion 16 of *Siemens* was used to perform the CT scan acquisitions during the core flooding tests. The CT scans were planned as a function of the Injected Pore Volume (PV_{inj}). The space interval between slices was of 10 mm. The energy used was 130 kVA, a pitch of 1 and repeatability of ±1 CT number. The image treatment was done using the software Image J-Fiji.

For calculating the saturation of fluids based on the CT monitoring were used the mathematic expressions proposed by Alvestad *et al.* (1992) [19] named CT_1, Sharma *et al.* (1997) [22] named CT_2, Chakravarthy *et al.* (2004) [23] named CT_3. The CT profiles of the references media *i.e.*, the (measured) rock saturated with brine and the (calculated) rock saturated with oil for each step are presented in Figure 2.

Besides that, aiming to obtain much more suitable images for rendering in 3D results, the data was smoothed using a Fast Fourier transform bandpass filter in a similar way that other authors [24].

3 Results and discussions

3.1 Dry rock sample CT evaluation

In this step, the CT scanner was used as a useful tool to visualize inside the core holder and to characterize the internal structure of 12A2 and 12A4 rock samples. The 12A4 dry rock sample was scanned with CT perceiving a longitudinal lamination in all slices characterized by a higher CT number distribution along it (green lamination in Figs. 3a and 3b). Denser materials are associated with these green marks. Probably, this lamination includes high clay content, since cement generates high CT number response. A 3D images reconstruction confirmed the presence of this structure throughout the entire rock sample length (Fig. 3c).

Although both rock samples used for the core-flooding tests exhibited thin laminations, we considered that the flow behavior was not disturbed because the laminations were in the same direction as the fluids flooding. Besides that, the rocks showed similar porosity and permeability values, and similar mineralogical composition. For future studies, we recommend doing a passive tracer test before running imbibition processes to assess the impact of the rock heterogeneity on fluids flow performance. That has already been done displacing undoped brine by doped brine [41].

3.2 Core flooding tests

This section encompasses the analyses of the results obtained for the core flooding proposed Test 1 – Waterflooding (WF), Test 2 – SP as a secondary recovery method and Test 3 – SP as a tertiary oil recovery method. Where is used the 2D and 3D imaging analyses to understand the phenomena acting inside the porous media and how they impact the oil recovery efficiency.

During Test 1 (Tab. 3), first, the absolute permeability of the rock sample 12A4 was determined by water injection (Imbibition) corresponded to 260.9 mD. This value was smaller than the value obtained during petrophysical characterization (gas permeameter) probably due to clays swelling present in the rock when they were exposed to a low salinity brine, fines migration or Klinkenberg effect.

Another useful application of the CT acquisition was the determination of the porosity profile throughout the rock sample before and after the Imbibition. These results were compared with the value determined using a gas porosimeter. Figure 4 summarizes these results.

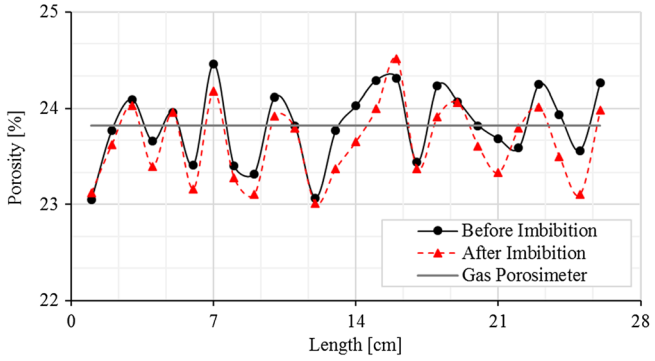

Fig. 4. Comparison of CT porosity profiles of 12A4 rock sample before imbibition 1, after imbibition 1 and gas porosimeter.

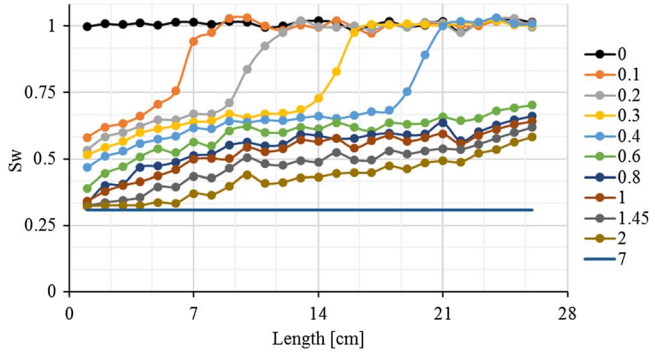

Fig. 5. Drainage 1 – water saturation profiles as a function of Injected Pore Volume (PV_{inj}) through rock sample 12A4.

The behavior of the porosity profile exhibits little changes throughout the rock, maybe because of the fines migration. Small particles can be removed and deposited in other parts or drained out of the rock sample. These changes are minor and can be disregarded since the tendency of the profile was maintained. The major utility of porosity results obtained with CT data is based on the creation of 2D porosity map of the rock sample and then, through a porosity-permeability correlation for this particular rock type create a 2D permeability map aiming to improve the numerical simulation of these core flooding tests [41].

After Imbibition, the oil injection starts, attempting to mobilize all of the existent mobile water inside the rock and establishing the initial reservoir conditions (S_{wi} and S_o). A total of 7.08 PV of oil were injected. The breakthrough (BT) of oil occurred when 0.56 PV had been injected. At the BT instant, about 81.58% of the total mobile water had been produced.

The water displacement up to the oil BT was developed with a homogenous advanced front due to the favorable mobility ratio between the fluids ($\mu_o > \mu_w$). This behavior can be observed with the water saturation profiles obtained by the CT scan (Fig. 5).

After the oil BT, the water saturation profile exhibited smaller values close to the inlet and higher ones near to the outlet face. It means that even though before the BT the displacement front was more like a piston, some oil flowed through preferential channels. After 6 PV of oil injected, the system was considered under steady-state flow regime, *i.e.*, there was no water production.

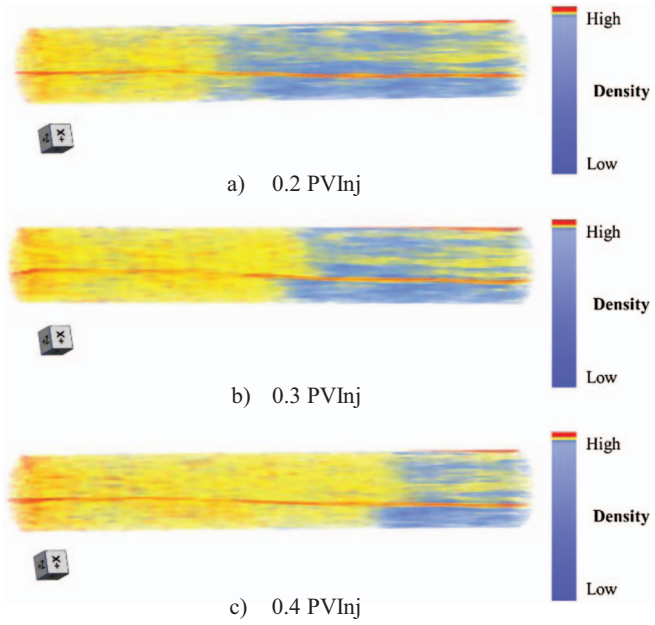

Fig. 6. Drainage 1 – 3D images in function of PV_{inj}. The color yellow, blue and red correspond to oil, water location and rock lamination, respectively.

Figure 6 presents 3-D reconstructions of the CT images up to 1 PV_{inj}. The green color represents the spatial distribution of the high CT number associated with the doped oil and the rock lamination previously mentioned, the blue color represents the water. These images confirmed that before BT, some significant amount of oil is accumulating close to the outlet rock face, *i.e.*, some oil droplets were transported and settled down with more frequency closer than the outlet face of the rock sample. However, the oil located there needs to reach the critical saturation to flow.

Since the rock was saturated according to initial reservoir conditions (S_{wi} and S_o), we started the assessment of the water injection as a secondary recovery method. A total of 15 PV of water were injected. The water BT occurred when 0.07 PV had been injected. At the BT of water, around 17.43% of the initial mobile oil had been produced.

The fact that a significant oil production occurred after the water BT shows the existence of preferential flow channels. The analysis of water saturation profiles as a function of the injected PV of fluid (Fig. 7) confirmed this phenomenon. These profiles exhibit a higher water saturation at the beginning and end of the rock sample while for a length between 10 cm and 20 cm the water saturation is lower and even in some sections continues being near to initial water saturation. *i.e.*, at the BT instant, a significant amount of oil has not been mobilized in these zones, yet.

Then, an increment on water saturation along the sample becomes more noticeable at one injected PV. The oil trapped close to the outlet face was produced and, at three

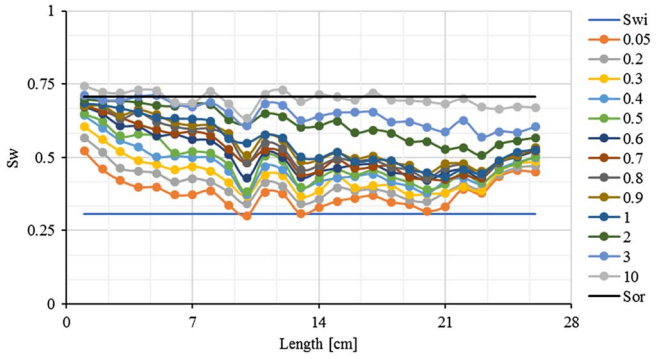

Fig. 7. Waterflooding – water saturation profiles as a function of Injected Pore Volume (PV_{inj}) through rock sample 12A4.

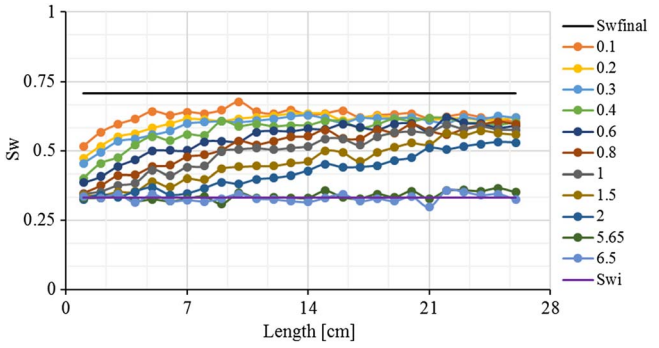

Fig. 9. Drainage 2 – water saturation profiles in function of Injected PV through rock sample 12A4.

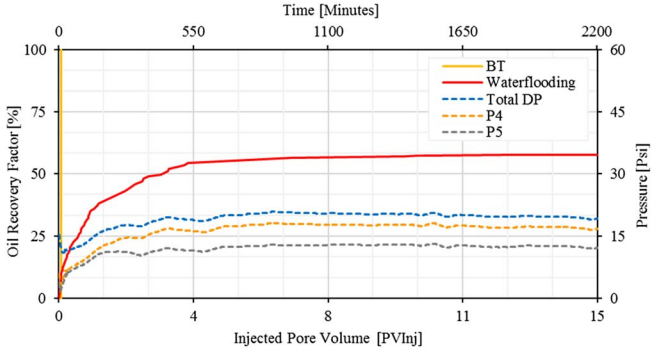

Fig. 8. Waterflooding – oil recovery factor and historical pressure in function of the PV_{inj} and time.

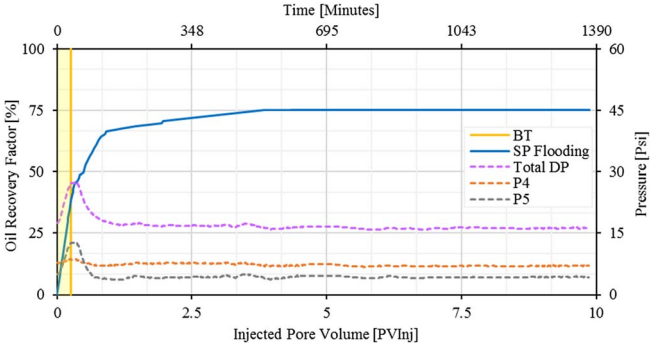

Fig. 10. CEOR process – oil recovery factor and historical pressure in function of the PV_{inj} and time.

injected PV, the saturation distribution became more homogenous. However, the water saturation remained higher at the injection face. Finally, after the injection of 10 PV, some local differences in oil saturation remained along the core sample, which was removed by the water injection up to 15 PV. Figure 8 shows that the final oil RF of the WF was 57.57%.

This figure also exhibits pressure behavior. The pressure drops until water BT, as it was expected. After that, the pressure increases due to water challenging to displace the high quantity of mobile oil remaining in the rock occasioned by oil still trapped inside the rock.

During Test 2 (Tab. 3), the rock sample was restored to a similar condition of the initial oil reservoir conditions (S_{wi} and S_o). A total of 7.39 PV of oil were injected. The BT of oil occurred when 0.08 PV of fluid had been injected. At the BT instant, about 12% of the mobile water had been produced. After BT the water production continued until approximately 5.6 PV_{inj} of oil. The water saturation profiles obtained by CT through the rock sample during the second drainage are presented in Figure 9. After the injection of 0.1 PV, all sections of the sample presented a water saturation below the initial value, confirming the fast BT of oil. The initial saturation profiles had a notable difference in the first 5 cm of the rock sample by the proximity to input diffuser as is expected.

The last three CT acquisitions showed a homogenous water distribution above 5.65 PV of oil injected, allowing affirming that the residual water in the porous media was immobile.

Then, the Surfactant/Polymer injection as a secondary oil recovery method started. A total of 10 PV of the chemical solution were injected. In this case, the stop criterion was a null oil production and a stabilization of the differential pressure to guarantee a residual oil saturation within the rock.

The BT of the chemical blend occurred when 0.26 PV had been injected. At BT, about 51.26% of the initial mobile oil was produced. After BT there was a continuous two-phase production until about 3.84 injected PV of SP blend. This production period was characterized by a high water volume production ($W_{cut} > 90\%$).

The total differential pressure having a progressive increment accompanied by a continuous oil production until the chemical BT (Fig. 10). After it, the pressure begins to fall to stabilize as it was expected. However, only the P5 presented a similar response to it. Maybe, the P4 transducer record failed during this phenomenon. Despite the above, the use of a blend of SP allowed achieving a final oil RF of 75%.

Figure 11 shows the chemical saturation profiles, where one can notice two relevant facts. The first of them (red arrow number 1) occurs around 0.1 and 0.2 PV of the chem-

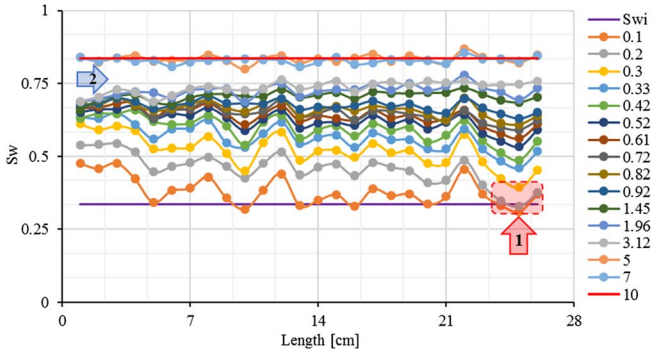

Fig. 11. CEOR process – water saturation profiles in function of PV_{inj} through rock sample 12A4.

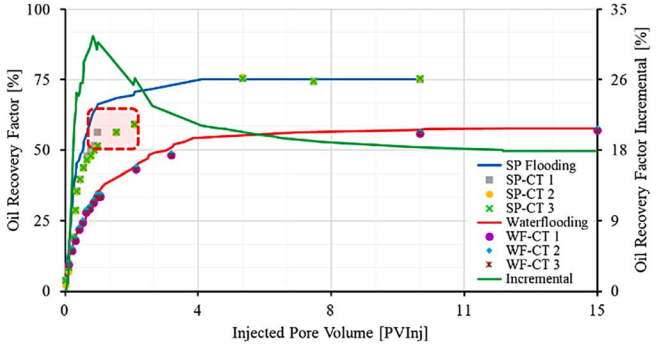

Fig. 12. Comparison of oil recovery factor obtained through volumetric material balance (continuous lines) and CT monitoring (dots) for WF and SP as secondary recovery methods.

ical injection. That occurrence can be explained by a significant amount of oil removed from the initial rock region and is driving by a microemulsion phase, which is not flowing easily, probably because it has a high viscosity [38].

The second fact detected in Figure 11 (blue arrow number 2) occurred during the higher microemulsion production and it will be commented later in Figure 12.

An oil RF performance comparison between the results obtained through CT saturation monitoring and volumetric material balance is shown in Figure 12 where is exhibited good matching during the waterflooding. However, in the SP injection, the red square emphasizes discrepancies (second fact exposed previously). The oil saturation in the plug as measured with CT scan appears higher than indicated from the volumetric material balance. Despite the above, the final oil recovery is similar to both measuring methods.

CT scan measurements cannot fail if we assume that the microemulsion is a mixture of the two phases taken as references (oil + iododecane on one side, brine + SP on the other side). Therefore, the discrepancy could then indicate a separation of a part of the iododecane in the mixture when contacting the SP solution and higher retention of the separated fraction of iododecane in the plug. Based on this, a iododecane fraction (far lower than 10% which is the initial fraction of iododecane in oil) generates very high

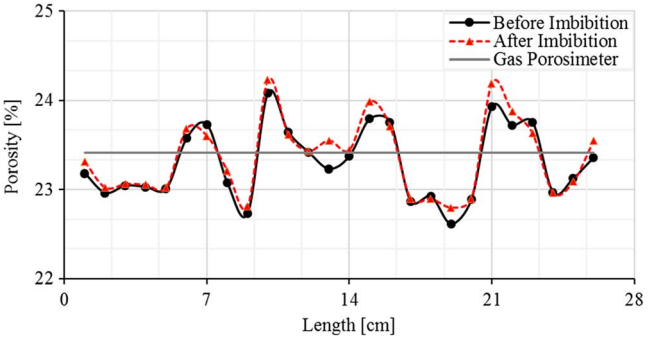

Fig. 13. Comparison of CT porosity profiles of 12A2 rock sample before imbibition, after imbibition and gas porosimeter.

CT values explaining that the phenomenon is not seen by material balance measurement.

In order to improve CT scan measurements, we suggest to use 3-phase calculation with three initial references (oil, iododecane and SP) or avoid marking the oil but in both cases, the accuracy of the measurements would be highly decreased. It is worth it to notice that the final recovery is the same whether calculated with volumetric material balance and CT saturation monitoring, even with the 2-phases calculations [19, 22, 23] showing that the iododecane separated fraction is finally produced in the same manner than the oil. Therefore, CT measurements remain reliable and accurate concerning the end points of a SP injection as a secondary oil recovery method.

Figure 12 also shows the difference in the oil RF between both secondary oil recovery processes (WF and SP). The highest efficiency of the SP process occurs at approximately 0.7 PV_{inj} obtaining 30% of incremental oil related to the same water volume used by WF method. After 0.7 PV_{inj}, the process efficiency starts to decrease and finally stabilizes around 17%.

The discussion above does not imply that a continuous SP injection is required to improve oil recovery significantly. If a small quantity of chemical (0.7 PV) was used alternating with the water injection, an improvement lower than 17% on the final WF oil RF could be obtained. This thesis motivated the assessment of tertiary flooding (Test 3) following presented.

The CT_1, CT_2 and CT_3 are compared in Figure 12. During the waterflooding the CT_2 exhibits a better fit with the volumetric material balance due to the correction by S_{wc} included in the mathematic expression proposed [22]. For the SP process the CT_1, CT_2 and CT_3 expression are able to give a good fit only at the initial and final saturations.

Thus, the execution of Test 3 starts with the absolute permeability of the rock sample 12A2 determination. The permeability corresponded to 287.7 mD. Also, the porosity profile of the 12A2 rock sample was determined by the CT, demonstrating since again, the CT accuracy for this application.

Comparing the porosimeter value and tomographic results (Fig. 13), one can observe that the behavior before and after K_w determination maintains the profile trend and does not present significant changes.

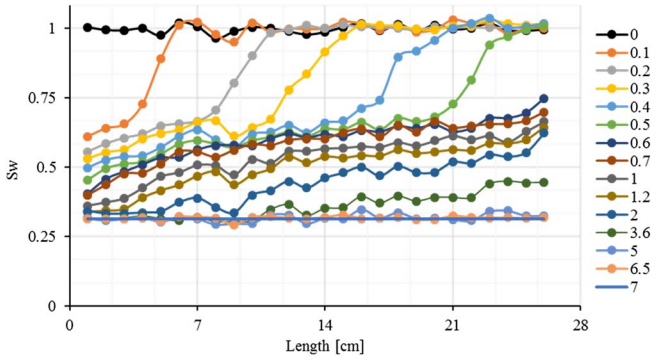

Fig. 14. Drainage – water saturation profiles in function of Injected Pore Volume (PV_{inj}) through the rock sample 12A2.

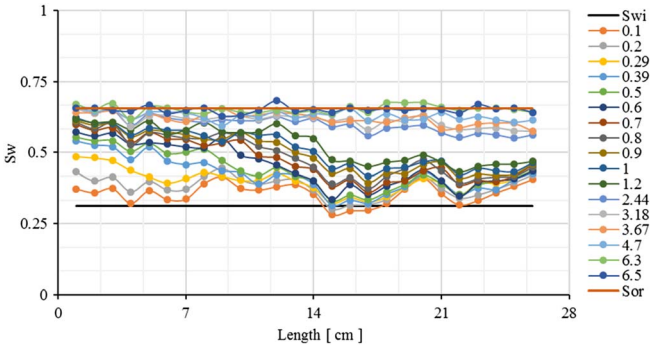

Fig. 15. Waterflooding – water saturation profiles in function of Injected Pore Volume (PV_{inj}) through rock sample 12A2.

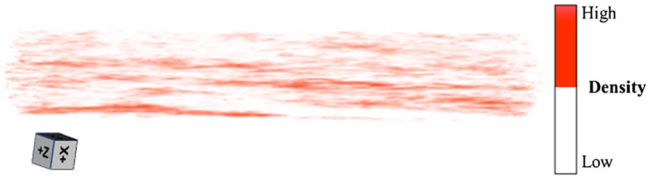

Fig. 16. Dry rock sample 12A2: 3D representation where the red color represents the laminations and high-density materials.

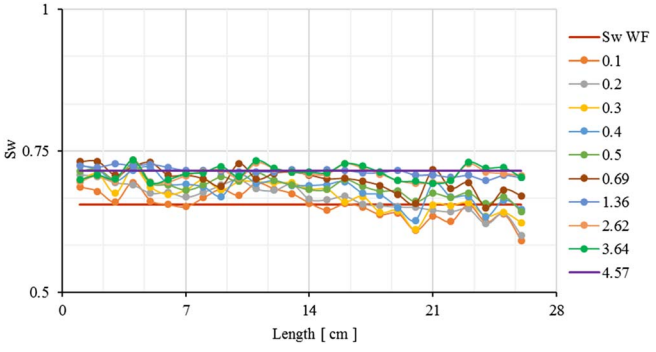

Fig. 17. CEOR 1 – water saturation profiles in function of PV_{inj} through rock sample 12A2.

After the Imbibition, a total of 7.13 PV of oil were injected aiming to displace all the existent mobile water inside the rock and restore the initial rock reservoir conditions. The BT of oil occurred at 0.59 PV_{inj}. At the BT instant, about 86% of the mobile water had been produced. The displacement of fluids until BT was performed with a homogenous advance front. This is confirmed by the water saturation profile obtained through CT technique (Fig. 14). When 3.6 PV of oil had been injected, the water saturation profile started to stabilize and finally, it presented homogeneous distribution through the rock sample when 6.5 PV of oil or more were injected.

Since the rock has been reestablished to initial reservoir conditions (S_{wi} and high S_o), the assessment of the Surfactant/polymer injection as a tertiary method supported by CT, started. First, a total of 6.71 PV of brine were injected. This amount was determined based on the results reported previously which the oil recovery performance during the waterflooding not exhibited significant changes after 7 PV_{inj} of water, and the W_{cut} was higher than 90%. The BT of brine occurred when 1.1 PV of fluid had been injected. At the brine BT, about 16% of the initial oil had been produced. The oil RF due to waterflooding stabilized in 49.95% with a W_{cut} of 94.88% by the end of the brine injection.

The CT saturation monitoring allowed determining of Figure 15. As the water injection progresses, there is a continuous increase of the water saturation at the region close to the inlet face of the rock sample.

After the middle of the rock, the water saturation does not present significant changes until 1.2 PV_{inj} due to the rock heterogeneity (Fig. 16). This heterogeneity creates a gap in the saturation profiles which was filled at 2.44 PV_{inj} of water, *i.e.*, before this instant, the water was heterogeneously distributed inside the rock sample. However, after 6 PV_{inj}, the water tends to be homogeneously distributed inside the porous media.

Despite the similar petrophysical and initial drainage performance between 12A2 and 12A4 rock samples, the usage of CT scanner as a tool to evaluate this core flooding test allows affirming that, the performance and displacement efficiencies during the waterflooding were different due to the internal rock heterogeneities. These heterogeneities dominated the fluids dynamics through preferable flow paths across the 12A2 rock sample.

Table 4. Average saturation values in function of PV_{inj} of CEOR 1 determined by CT monitoring.

PV_{inj}	0.1	0.2	0.3	0.4	0.5
S_w	0.655	0.667	0.672	0.684	0.687
S_o	0.345	0.333	0.328	0.316	0.313

After the brine injection, CEOR processes are applied and evaluated by CT. It consisted of two slugs of SP blend kept separated by a brine drive fluid. In the first chemical slug, a total 0.69 PV of SP blend were injected. This slug broke through after 0.26 PV_{inj}. The amount of the first chemical slug was chosen as the quantity of SP blend which the process presented the highest efficiency during Test 2, corresponding to 0.7 PV (Fig. 12). This stage was named CEOR1 (Tab. 3).

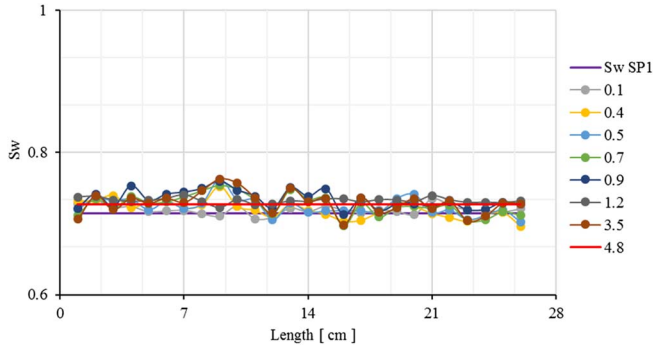

Fig. 18. CEOR 2 – water saturation profiles as a function of PV_{inj} through rock sample 12A2

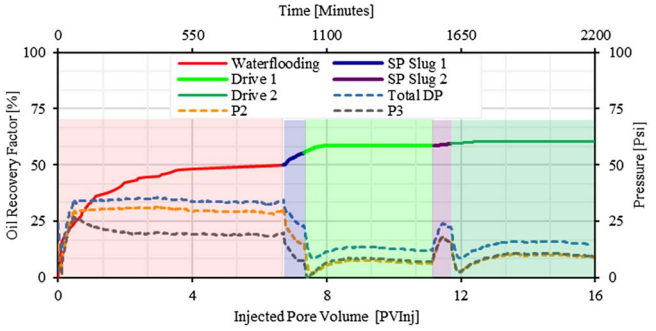

Fig. 19. Test 3 – oil recovery factor performance and Historical pressure as a function of PV_{inj} and time.

Table 5. Average saturation values in function of PV_{inj} of CEOR 2 determined by CT monitoring.

PV_{inj}	0.1	0.4	0.5	3.5
S_w	0.719	0.720	0.724	0.729
S_o	0.281	0.280	0.276	0.271

After having injected 3.88 PV of drive brine, the second chemical slug started, and a total of 0.53 PV of SP blend were used. This slug reached the outlet face after 0.33 PV_{inj}. Finally, a total of 4.27 PV of brine were used as the second drive fluid. This stage was named CEOR 2 (Tab. 3).

Figure 17 shows the CT saturation monitoring results during CEOR 1 process. The fact that the profiles between 0.1 and 0.5 PV_{inj} got out the lower limit established by the volumetric MB is not a numerical mistake or a limitation of the CT.

This behavior is characterized by the increases in the average value of S_w and therefore, a decrease in the average value of S_{or} through the rock (Tab. 4). In fact, it is a response to the mobilization of the residual close to the inlet face of the rock and their displacement throughout the sample.

During CEOR 2 stage, the water saturation distributions got out the upper limit established by the volumetric MB due to since additional oil is mobilized by the second SP slug injected (Fig. 18).

Part of this incremental oil is then moved, and part remains inside the pores close to the outlet face. The average values of fluids saturation calculated by CT confirm this behavior (Tab. 5).

Figure 19 presents the histories for oil recovery and differential pressure of Test 3. Based on those results, it is possible to conclude that each recovery method achieved a S_{or} condition because a pressure history and oil RF plateaus are reached before the next stage starts. Besides that, an incremental reduction of the previous residual oil saturation was obtained by the subsequent process ($FR_{WF} < FR_{CEOR\ 1} < FR_{CEOR\ 2}$).

An oil RF performance comparison between the results obtained through CT saturation monitoring and volumetric material balance is shown in Figure 20.

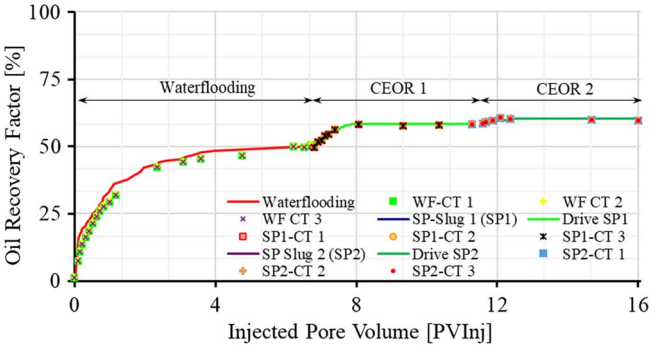

Fig. 20. Comparison of oil recovery factor obtained through volumetric material balance (Continuous lines) and CT monitoring (Dots) for SP process as tertiary oil recovery method.

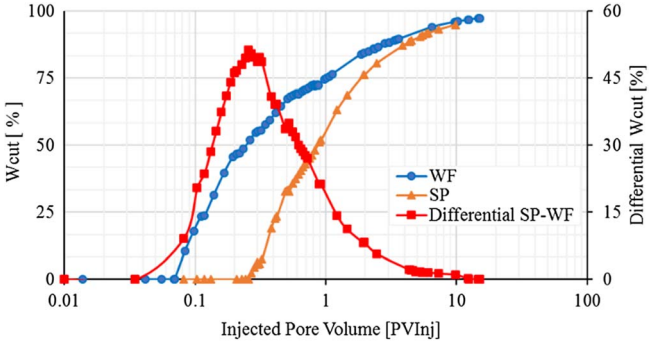

Fig. 21. W_{cut} comparison between WF (Test 1) and SP as a secondary process (Test 2). Also, it is shown the differential W_{cut}.

Comparing the results obtained through CT saturation monitoring and volumetric material balance is provided a good agreement for both process (WF and SP) using any of the mathematical expressions used (CT_1, CT_2 and CT_3). This matching demonstrates the utility of the CT tool to improve the understanding of the fluids dynamics in porous media when the microemulsion within the rock does not reach a significant amount, and therefore, the water and oil volumes in each pixel of the image are accurately quantified through the CT.

Table 6. Comparative results of mobility control improvement on some properties during the assessment of secondary injection schemes.

Property	Secondary injection schemes		
	WF	SP blend	Comments
Initial oil saturation (S_{oi})	0.69	0.67	Similar drainage cycles
VP_{Inj} up to BT	0.07	0.26	Breakthrough delay: mobility control
RF up to BT	10.1	38.5	IFT reduction and displacement efficiency improvement
PV_{inj} up to W_{cut} of 80%	1.5	2.46	Water production management
RF up to W_{cut} of 80%	40.8	71.8	IFT reduction and displacement efficiency improvement
PV_{inj} up to W_{cut} of 95%	9.6	9.96	Similar behavior at high quantities of injected fluids
RF up to W_{cut} of 95%	56.8	0.75	IFT reduction and displacement efficiency improvement
RF at final of the test	57.8	0.75	SP blend usage improves the process efficiency
Residual oil saturation (S_{or})	0.29	0.17	High oil saturation reduction (40% lower)

Table 7. Comparative results of mobility control improvement on some properties during the assessment of tertiary injection schemes.

Property	Tertiary injection schemes			
	WF	SP blend		Comments
		CEOR 1	CEOR 2	
Initial oil saturation (S_{oi})	0.69	0.34	0.29	
VP_{Inj} up to BT	0.11	0.26	0.30	Breakthrough delay: mobility control
RF up to BT	16.03	+2.01	+0.27	IFT reduction and displacement efficiency improvement
PV_{inj} up to W_{cut} of 80%	1.48	–	–	
RF up to W_{cut} of 80%	38.2	–	–	
PV_{inj} up to W_{cut} of 95%	6.8	1.36*	–	*Slight water production management
RF up to W_{cut} of 95%	49.95	+8.48	–	IFT reduction and displacement efficiency improvement
RF at final of the test	49.95	+8.48	+1.91	SP blend slugs improve the process efficiency
Residual oil saturation (S_{or})	0.34	0.29	0.27	Oil residual saturation reduction in each step

An oil recovery incremental of 10.39 percentage points compared to WF could be obtained using the surfactant/polymer blend proposed as a tertiary oil recovery method under the tested conditions. Nevertheless, a CEOR process is more efficient when is used in early stages during field development.

3.3 Other comparisons of tests results

W_{cut} of Test 1 and Test 2 are analyzed aiming to stand out the main differences between both processes.

Figure 21 presents the W_{cut} comparisons showing an initial reduction of the amount of produced water as a result of a better mobility ratio of the SP process. These results are evidenced by a delay in the breakthrough of the chemical injected fluid when comparing the SP and the WF. The lower W_{cut} continues until approximately 5 PV_{inj} of the SP blend. After that, the W_{cut} tends to be very similar for both processes, because the majority of the recoverable oil had already been produced.

Tables 6 and 7 show the comparative results of each injection scheme. Those results demonstrate the mobility control improvement exercised for the SP blend on different flow properties.

4 Conclusion

Regarding the effectiveness of the CT for the experimental assessment of SP flooding, it is concluded that:

The use of the CT scanner during core-flooding tests is a powerful tool to determine the porosity and saturation profiles along the rock sample. Also, visualization inside of the rock (2D and 3D) improves the two-phase flow dynamic understanding through the porous media.

A misfit between oil recovery performance obtained through volumetric material balance and CT monitoring was identified when conducting the SP process as a secondary oil recovery method (S_{wi} and high S_o) at the tested conditions. Since there is a good matching between both methods during the waterflooding, CT scan measurements cannot fail if we assume that the microemulsion is a mixture of the 2 phases taken as references (oil + iododecane on one side, brine + SP on the other side).

The discrepancy could then indicate a separation of a part of the iododecane when contacting the SP solution and higher retention of the separated fraction of iododecane in the plug. Despite the above, the final oil recovery is the same whether calculated with volumetric material balance and CT saturation monitoring, even with the 2-phases calculations showing that the iododecane separated fraction is finally produced in the same manner as the oil with some delay. Therefore, CT measurements remain reliable and accurate concerning the end points of a SP injection as a secondary oil recovery method.

For the assessment of SP blend processes as tertiary oil recovery methods, the CT was an accurate tool to determine the volume fraction of the fluids inside the rock.

Finally, based on the core-flooding tests evaluated through CT and material balance comparative analysis of the SP flooding as secondary and tertiary oil recovery methods, it is concluded that:

The SP blend used as a secondary and tertiary oil recovery method provided an improvement in the oil RF of 17 and 10 percentage points compared to the conventional waterflooding.

The SP blend generates a better mobility ratio, which was evidenced by the delay of the breakthrough respect to the conventional waterflooding.

The water–oil ratio during the CEOR processes diminished due to the improvement of displacement efficiency and mobilization of the residual oil saturation.

CEOR methods are more efficient when they are applied in early stages during the field development as a strategy of field management.

Acknowledgments. The authors wish to thank the Coordenação de Aperfeiçoamento de Pessoal de Nível Superior (CAPES) and, the Department of Energy DE-FEM-UNICAMP for their support of this work.

References

1 British Petroleum BP statistical review of world energy statistical review of world, *Ed. BP Stat. Rev. World Energy* 1–69.

2 Sheng J.J. (2013) *Enhanced oil recovery field case studies*, Gulf Professional Publishing, 712 p.

3 Lake L.W. (1991) *Enhanced oil recovery*, Facsimile (ed), Prentice-Hall, Englewood Cliffs.

4 Taber J.J., Martin F.D., Seright R.S. (1997) EOR screening criteria revisited – Part 1: Introduction to screening criteria and enhanced recovery field projects, *SPE Reserv. Eng.* **12**, 3, 189–198.

5 Shandrygin A., Lutfullin A. (2008) Current status of enhanced recovery techniques in the fields of Russia, *SPE Annu. Tech. Conf. Exhib.*, 1–24 September, Denver, Colorado, USA, pp. 21–24.

6 Healy R.N., Reed R.L. (1974) Physicochemical aspects of microemulsion flooding, *Soc. Pet. Eng. J.* **14**, 5, 491–501.

7 Stoll W.M., Al-Harthy S.A.A., Van Wunnik J., Faber M.J. (2011) Alkaline/surfactant/polymer flood: From the laboratory to the field, *SPE Reserv. Eng.* **14**, 6, 702–712.

8 Batenburg D.W., Berg S., Oedai S., Elewaut K. (2015) Visualization of oil mobilization in ASP core floods using X-ray CT imaging, *SPE Kuwait Oil and Gas Show and Conference*, 11–14 October, Mishref, Kuwait.

9 London M., Cameron S.M., Donald J., Wassmuth F.R. (2014) Waterflooding experiments with X-ray CT imaging, *SPE Heavy Oil Conference-Canada*, 10–12 June, Calgary, Alberta, Canada, pp. 1–15.

10 Hove A., Nilsen V., Leknes J. (1990) Visualization of xanthan flood behavior in core samples by means of X-ray tomography, *SPE Reserv. Eng.* **5**, 4, 475–480.

11 Hunt P.K., Engler P., Bajsarowicz C. (1988) Computed tomography as a core analysis tool: Applications, instrument evaluation, and image improvement techniques, *J. Pet. Technol.* **40**, 09, 1203–1210.

12 Wang S., Ayral S., Gryte C. (1984) Computer-assisted tomography for the observation of oil displacement in porous media, *Soc. Pet. Eng. J.* **24**, 1, 53–55.

13 Wellington S.L., Vinegar H.J. (1987) X-ray computerized tomography, *J. Pet. Technol.* **39**, 08, 885–898.

14 Vinegar H.J., Wellington S.L. (1987) Tomographic imaging of three-phase flow experiments, *Rev. Sci. Instrum.* **58**, 1, 96–107.

15 Withjack E.M. (1988) Computed tomography for rock-property determination and fluid-flow visualization, *SPE Form. Eval.* **3**, 696–704.

16 Withjack E.M., Devier C., Michael G. (2003) The role of X-ray computer tomography in core analysis, *SPE West. Reg. Pacific Sect. Jt. Meet.*, 19–24 May, Long Beach, CA, USA, pp. 12. No. SPE Paper #83467.

17 Wan T., Yang S., Wang L., Sun L. (2019) Experimental investigation of two-phase relative permeability of gas and water for tight gas carbonate under different test conditions, *Oil Gas Sci. Technol. - Rev. IFP Energies nouvelles* **74**, 23.

18 Ouali C., Rosenberg E., Barré L., Bourbiaux B. (2019) A CT-scanner study of foam dynamics in porous media, *Oil Gas Sci. Technol. - Rev. IFP Energies nouvelles* **74**, 33.

19 Alvestad J., Gilje E., Hove A.O., Langeland O., Maldal T., Schilling B.E.R. (1992) Coreflood experiments with surfactant systems for IOR: Computer tomography studies and numerical modelling, *J. Pet. Sci. Eng.* **7**, 1–2, 155–171.

20 Coles M.E., Muegge E.L., Auzerais F., Frulla P., Kantzas A. (1995) The use of attenuation standards for CT scanning, *SCA Conference*.

21 Hicks P.J. (1996) X-ray computer-assisted tomography for laboratory core studies, *J. Pet. Technol.* **48**, 12, 1120–1122.

22 Sharma B.C., Brihgam W.E., Castainer L.M. (1997) *CT imaging techniques for two-phase and three-phase in-situ saturation measurements*, Tulsa.

23 Chakravarthy D., Muralidharan V., Putra E., Schechter D.S. (2004) Application of X-ray CT for investigation of CO_2 and WAG injection in fractured reservoirs, *Petroleum Society's 5th Canadian International Petroleum Conference*, pp. 1–14.

24 Berg S., Oedai S., Landman A.J., Brussee N., Boele M., Valdez R., van Gelder K. (2010) Miscible displacement of oils by carbon disulfide in porous media: Experiments and analysis, *Phys. Fluids* **22**, 11, 113102.

25 Berg C.F., Lopez O., Berland H. (2017) Industrial applications of digital rock technology, *J. Pet. Sci. Eng.* **157**, 131–147.

26 Berg S., Ott H. (2012) Stability of CO_2 – Brine immiscible displacement, *Int. J. Greenh. Gas Control* **11**, 188–203.

27 Carcoana A.N. (1982) Enhanced oil recovery in Rumania, *SPE Enhanced Oil Recovery Symposium*, 4–7 April, Tulsa, Oklahoma. SPE-10699-MS.

28 Goodlett G., Honarpour M.M., Chung F.T. (1986) The role of screening and laboratory flow studies in EOR process evaluation, *SPE Rocky Mountain Regional Meeting*, 19–21 May, Billings, Montana, pp. 28.

29 Brashear J.P., Kuuskraa V.A. (1995) The potential and economics of enhanced oil recovery, *J. Pet. Technol.* **30**, 9, 1231–1239.

30 Al-Bahar M.A., Merrill R., Peake W., Jumaa M., Oskui R. (2004) Evaluation of IOR potential within Kuwait, *Abu Dhabi International Conference and Exhibition*, 10–13 October, Abu Dhabi, United Arab Emirates.

31 Ezekwe N. (2011) *Petroleum reservoir engineering practice*, Pearson Education Inc., Boston.

32 Sheng J.J. (2015) Status of surfactant EOR technology. *Petroleum* **1**, 2, 97–105.

33 Suarez A.F., Gaviria W., Pavas J., Frorup M.D. (2005) Beating the marginal well performance in a mature field: San Francisco Field in Colombia, *SPE Lat. Am. Caribb. Pet. Eng. Conf.*, 20–23 June, Rio de Janeiro, Brazil.

34 Claes S., Nader F.H., Youssef S. (2018) Coupled experimental/numerical workflow for assessing quantitative diagenesis and dynamic porosity/permeability evolution in calcite-cemented sandstone reservoir rocks, *Oil Gas Sci. Technol. - Rev. IFP Energies nouvelles* **73**, 36.

35 De Melo M., Lucas E. (2008) Characterization and selection of polymers for future research on enhanced oil recovery, *Chem. Chem. Technol.* **2**, 4, 295–303.

36 Sanabria F.C.B. (2013) *Avaliação da injeção de surfactantes como método de recuperação avançada em reservatórios de arenito*, São Paulo.

37 API (1990) *Recommended practices for evaluation of polymers used in enhanced oil recovery operations*, Washington, p. 86.

38 Tapias Hernández F.A., Moreno R.B.Z.L. (2019) Assessment of a surfactant-polymer formulation applied to the conditions of one, *CT & F – Ciencia Tecnol. y Futur.* **9**, 47–63.

39 Dos Santos R.L.A., Bedrikovetsky P., Holleben C.R. (1997) Optimal Design and Planning for Laboratory Corefloods, *Latin American and Caribbean Petroleum Engineering Conference*, 30 August–3 September, Rio de Janeiro, Brazil. SPE 39038.

40 Bonilla Sanabria F.C., Moreno R.B.Z.L. (2013) Surfactant flooding evaluation for enhanced oil recovery in sandstones reservoirs, *European Symposium on Improved Oil Recovery.*

41 Berg S., Oedai S., Ott H. (2013) Displacement and mass transfer between saturated and unsaturated CO_2-brine systems in sandstone, *Int. J. Greenh. Gas Control* **12**, 478–492.